Research Square

Preprints are preliminary reports that have not undergone peer review.
They should not be considered conclusive, used to inform clinical practice,
or referenced by the media as validated information.

Antiferromagnetic Pure Spin Current Memdevices

Martin Latorre
University of Chile
Gaspar De la Barrera
Johannes Gutenberg University Mainz
Roberto E. Troncoso
r.troncoso.c@gmail.com
University of Tarapacá
Alvaro S. Nunez
University of Chile

Article

Keywords: Antiferromagnetic spintronics, Pure spin current, Spin memristor, Piezospintronic effect

Posted Date: September 1st, 2026

DOI: https://doi.org/10.21203/rs.3.rs-10713844/v1

License: This work is licensed under a Creative Commons Attribution 4.0 International License.
Read Full License

Additional Declarations: No competing interests reported.

Antiferromagnetic Pure Spin Current Memdevices

Martin Latorre[1], Gaspar De la Barrera[2†], Roberto E. Troncoso[3*†], Alvaro S. Nunez[1†]

[1]Departamento de Física, Facultad de Ciencias Físicas y Matemáticas, CEDENNA, Universidad de Chile, Santiago,8370448, Chile.
[2]Institute of Physics, Johannes Gutenberg University Mainz, Mainz, 55099, Germany.
[3]Departamento de Física, Facultad de Ciencias, Universidad de Tarapacá, Arica, Casilla 7-D, Chile.

*Corresponding author(s). E-mail(s): r.troncoso.c@gmail.com;
Contributing authors: martin.latorre@ug.uchile.cl;
gdelabar@uni-mainz.de; asnunez@uchile.cl;
†These authors contributed equally to this work.

Abstract

Spin currents can be generated through various mechanisms, including the piezospintronic effect, which arises when strain or lattice distortions induce a change in the dipolar spin moment, causing a pure spin current without necessarily being accompanied by net charge transport. This opens new possibilities for low-power information processing and novel device architectures. In this work, we propose a novel effect, the spintronic-magneto-impedictive effect, as the theoretical basis for a pure spin-current memory-like device based on antiferromagnetic components. We focus on materials that can be modeled by the so-called spin-Rice-Mele Hamiltonian, incorporating a magnetic field gradient that explicitly breaks inversion symmetry. Our results shed light on how spin currents are generated and controlled, providing new insights into the potential of these materials for next-generation spintronic technologies.

Keywords: Antiferromagnetic spintronics, Pure spin current, Spin memristor, Piezospintronic effect

1 Introduction

Spin-currents are a central concept in spintronics [1–3], describing the transport of spin angular momentum through a material. In contrast to conventional charge currents, spin-currents are even under time reversal [4] and can propagate without an accompanying flow of net charge, thereby enabling fundamentally new paradigms for low-power information processing and spin-based device architectures. Spin-currents can be generated via spin polarized charge injection from ferromagnets [5], spin Hall and inverse spin Hall effects in materials with strong spin-orbit coupling [6], and dynamical processes such as spin-pumping [7] and the spin Seebeck effect [8]. They can be manipulated and detected through spin-orbit torques [9], nonlocal spin-valve geometries [10], and optical probes [11]. Beyond applications, spin-currents provide a versatile platform for exploring fundamental condensed-matter phenomena [12]. Their coupling to magnetization dynamics, quantum coherence, and topological electronic states continues to drive progress across a wide range of material systems, including transition-metal ferromagnets [13], heavy metals [14], topological insulators [15], and antiferromagnets [16].

Antiferromagnets are excellent platforms for spin transport because they combine zero net magnetization with strong spin dynamics [17–19]. Their compensated order suppresses stray fields and supports terahertz-speed dynamics, unlike ferromagnets. Spin currents in antiferromagnets (AFs) can be carried by itinerant electrons via spin-dependent scattering or by magnons. Their symmetry enables efficient spin–orbit-driven generation and detection of spin currents, while mitigating ferromagnetic drawbacks such as cross-talk and magnetic-field sensitivity. Moreover, AFs feature long spin diffusion lengths [20, 21] and support spin transport in both collinear and noncollinear textures, positioning antiferromagnetic spintronics as a fast-growing field for high-speed memory, logic, and low-power spin-based interconnects.

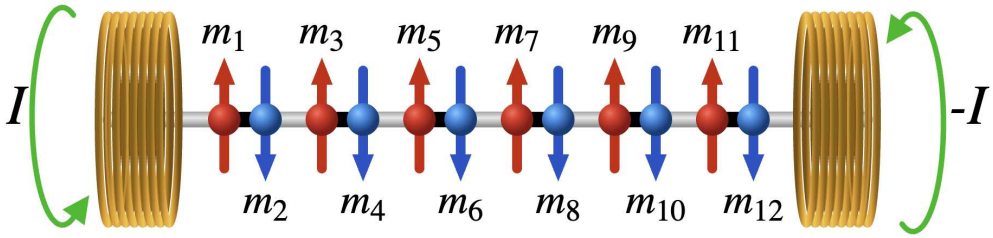


Fig. 1 Schematic setup for AF Rice-Mele spin chain subjected to a magnetic field gradient. Black and gray bonds represent the short and long links, respectively.

Recent studies show that certain AFs display a spin-dependent piezospintronic effect [22–27], where mechanical deformation in systems with coupled spin, lattice, and electronic degrees of freedom generates and controls spin currents. Analogous to the piezoelectric effect—where strain modifies electric polarization—the piezospintronic effect occurs when strain or lattice distortions induce a dipolar spin moment, producing a pure spin current without charge flow. This direct coupling allows mechanical control

of spin transport and accumulation, offering an alternative to electrical or thermal spin-current generation. The effect is especially strong in low-dimensional magnetic insulators, where nanoscale elastic deformations can be engineered, enabling flexible, low-power, multifunctional spintronic devices [25].

In this Letter, we propose a theoretical framework for a pure spin-current, memory-like device based on antiferromagnetic components [28–32]. The central prediction is the spintronic-magneto-impedictive effect, an impedance-like relation between spin-current and an external magnetic-field gradient, as illustrated schematically in Fig. 1. Our results advance the understanding of spin-current generation and control, shed light on the piezospintronic effect, and reveal new opportunities for harnessing spin-currents in next-generation spintronic technologies [33, 34].

2 Spintronic magneto-memimpedance

We consider a basic setup involving a $\mathcal{PT}$-invariant piezospintronic antiferromagnet, as in Ref. [22]. We show that, under a magnetic field gradient, the system emits a spin current that follows the linear-response relation

$$\mathbf{J}_S(\omega) = Z_S(\boldsymbol{\alpha}, \omega)\nabla B(\omega), \tag{1}$$

in frequency space, where Z_S is a pure spin-current magneto-memimpedance [35, 36], and $\boldsymbol{\alpha}$ denotes parameters characterizing the system state (e.g., the Néel vector or elastic strain). The parameters evolve in time according to $d\boldsymbol{\alpha}/dt = \mathcal{F}(\boldsymbol{\alpha}, \nabla B)$, with known $\mathcal{F}$, making these two equations analogous to those of a memristor [29]. Magnetic field–gradient control of magnetic excitations has previously been studied in the framework of magnetic straintronics [37–40].

The coupling to a field gradient produces three main effects: (i) a direct Zeeman action of ∇B on the dynamics of $\mathbf{n}$; (ii) a modification of the electronic spectrum that explicitly breaks inversion symmetry; and (iii) opposite forces on the two antiferromagnetic sublattices, causing a lattice distortion that reinforces dimerization. The memory in this device is stored in the time-dependent state of its Néel vector $\mathbf{n}$ and in the lattice distortion u. In this analogy, the read aspects of the memory are provided by the generated spin current. In a generic system, there are three contributions to $Z_S(\boldsymbol{\alpha}, \omega)$: the piezospintronic response $\lambda_{\mathrm{pzsp}} = \partial \mathbf{P}_S/\partial u$ [22], the Néel-vector modulation $\lambda_n = \partial \mathbf{P}_S/\partial n$, and the magnetization-gradient contribution $\lambda_{\nabla B} = \partial \mathbf{P}_S/\partial(\nabla B)$. They can be cast in the equation,

$$\mathbf{J}_S = \frac{d\mathbf{P}_S}{dt} = \lambda_{\mathrm{pzsp}}\frac{d\mathbf{u}}{dt} + \lambda_n \frac{d\mathbf{n}}{dt} + \lambda_{\nabla \mathrm{B}}\frac{d\nabla \mathbf{B}}{dt}. \tag{2}$$

Modeling the mechanical degrees of freedom as an overdamped particle subjected to the force $g\mu_B \nabla B$ [41–43], we obtain:

$$Z_S(\boldsymbol{n}, u, \omega) = (\mu\, \lambda_{\mathrm{pzsp}} + \nu\, \lambda_n) + i\, \omega\, \zeta\, \lambda_{\nabla \mathrm{B}}, \tag{3}$$

where the parameters μ, ν, and ζ, depend on the mechanical and magnetic states of the system.

3 Microscopic model

We now focus on certain materials that can be modeled by the so-called spin-Rice-Mele Hamiltonian [25, 44, 45]. Within this class of materials, we can find systems such as one-dimensional MoX_3 (X = Cl, Br, I) [46] and FeOOH [26]. The Hamiltonian for the system can be written:

$$\mathcal{H}_{\rm el} = -\sum_n \Big[\mathrm{t}_n(\mathbf{u})\, c^\dagger_{n+1,\sigma} c_{n,\sigma} + \mathrm{h.c.} \\ +(-1)^n c^\dagger_{n,\sigma} \left(\Delta \mathbf{n} \cdot \boldsymbol{\tau}_{\sigma\sigma'}\right) c_{n,\sigma'} \Big], \tag{4}$$

where $\mathbf{n}$ stands for the Néel vector of the antiferromagnetic chain. The dimerized hopping amplitude is $t_n(u) = t + (-1)^n \delta t(u)$, being the parameter $\delta t(u)$ dependent on the lattice deformation. Here u is the deviation of the dimerization from its equilibrium value u_0, i.e., the change in bond-length alternation within the unit cell; it is a scalar describing the relative shift of the two sublattice atoms along the chain. In line with standard Rice–Mele treatments with electron–phonon coupling, we set $\delta t(u) = \alpha_{\rm ep}\, u$, with $\alpha_{\rm ep}$ the electron–phonon coupling constant; this leading linear term for small u drives the Peierls instability. The spin polarization depends on time through $\mathbf{u}$ and $\mathbf{n}$. These, in turn, behave according to the classical overdamped equations [17, 47, 48],

$$\gamma \frac{du}{dt} + k(u - u_0) + g\mu_B\, n_z \nabla B = 0, \tag{5}$$

$$\mathbf{n} \times \left(m \frac{d^2\mathbf{n}}{dt^2} + \alpha_n \frac{d\mathbf{n}}{dt} - a_n \left(\mathbf{h_n} + g\mu_B (\nabla B) \hat{\mathbf{z}} \right) \right) = 0, \tag{6}$$

where k is the elastic constant of the material, γ is the damping coefficient of the lattice displacement, u_0 represents the dimerization at equilibrium, a_n is the homogeneous exchange coefficient, and h_n is the uniaxial anisotropy constant. The parameter $m = a_n h_n / \omega^2_{\rm AFMR}$ represents the effective inertia associated with the Néel order parameter, determined by a_n, h_n, and the antiferromagnetic resonance frequency $\omega_{\rm AFMR}$, while $\alpha_n = \sqrt{a_n h_n}/Q$ is the Néel damping parameter, characterizing the dissipation of the staggered order dynamics, with $Q = 10$ the quality factor of the antiferromagnetic resonance, and $\mathbf{h_n}$ the uniaxial anisotropy field. A magnetic-field gradient enters as a perturbation directed along the z-axis, $\nabla B\, \hat{\mathbf{z}}$, where $\nabla B = \partial_z B$, and contributes through a position-dependent Zeeman coupling. This term can be decomposed into (i) a contribution proportional to the spatial variation of the eigenstates and (ii) a sublattice-resolved coupling to the local spin moments. The resulting perturbation reads,

$$H_{\nabla B} = -g\mu_B (\nabla B) \sum_n \left[x_{nA} S^z_{nA} + x_{nB} S^z_{nB} \right], \tag{7}$$

where $g\mu_B$ is the effective magnetic moment, and the intra-unit-cell displacement β defines the sublattice positions $x_{nA} = na - \beta$ and $x_{nB} = na + \beta$. The spin operator

is given by $S^z_{ns} = (c^\dagger_{n,s}\sigma^z c_{n,s})/2$, with $s \in A, B$ and σ^z the z-component of the Pauli matrix vector. Equation (7) captures contribution (ii) explicitly; contribution (i) is implicitly accounted for through the first-order correction to the eigenstates, $|\psi^{(1)}_{-,\sigma}\rangle$, which enters the spin polarization P_S and governs the $\lambda_{\nabla B}$ coefficient in Eq. (10). The z axis is chosen along the direction of the applied magnetic-field gradient, which also coincides with the easy axis of the antiferromagnet. This perturbation provides a controlled, adiabatic modulation of the dimerization.

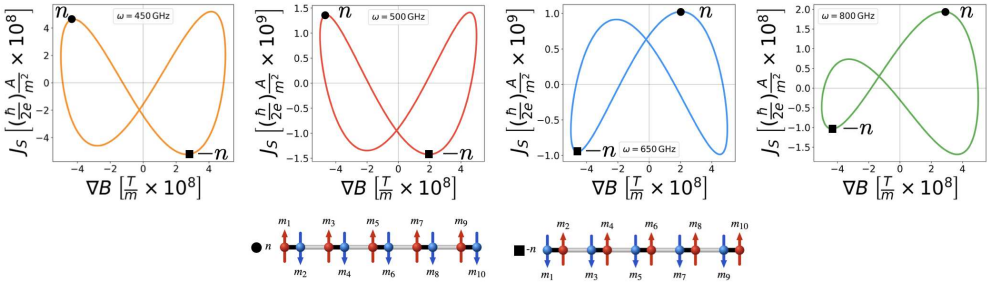


Fig. 2 Simulated spin-current curves as a function of the magnitude of the magnetic-field gradient applied to FeOOH chains, for driving frequencies of 450, 500, 650, and 800 [GHz] in panels (a)–(d), respectively. The magnetic-field gradient is of the order of $\nabla B = 10^8$ [T/m], which is within the experimentally relevant range [49].

4 Results

By analyzing the perturbative contribution $H_{\nabla B}$, it is necessary to treat the system response within the framework of degenerate perturbation theory, thereby obtaining the eigenvectors associated with this effect. The perturbation theory used to obtain the corrected eigenstates $|\psi_{-,\sigma}\rangle$ is static (time-independent), applied at each instant to the instantaneous Hamiltonian parametrized by $u(t)$ and $\mathbf{n}(t)$, following standard adiabatic treatments [50, 51]. The time dependence of J_S then enters entirely through the classical equations of motion for u and $\mathbf{n}$, Eqs. (5)–(6). One way to verify the existence of a significant effect arising from the inclusion of this term is to compute the spin polarization within linear response; for this purpose, we use:

$$\mathbf{P}_S = \sum_\sigma \frac{a}{2\pi} \int_{BZ} dk\, i\, \langle \psi_{-,\sigma} |\, \vec{\tau} | \partial_k \psi_{-,\sigma} \rangle$$

where $|\psi_{-,\sigma}\rangle = |\psi^{(0)}_{-,\sigma}\rangle + \nabla B |\psi^{(1)}_{-,\sigma}\rangle$, $\sigma \in \{\uparrow, \downarrow\}$ denotes the electron spin, and $\vec{\tau} = \vec{\sigma} \otimes \mathbb{1}$ is the sublattice operator with eigenvalues ± 1 corresponding to sublattices A and B. The subscript "$-$" labels the lower (valence) band of the Rice–Mele spectrum, which is fully occupied in the ground state; the upper (conduction) band carries the "$+$" label. Since only the valence band contributes to the ground-state spin polarization, only $|\psi_{-,\sigma}\rangle$ appears in the expression for P_S. In the antiferromagnetic ground state,

the Néel order couples spin to sublattice occupation, such that the contributions from spin-↑ and spin-↓ channels to P_S are finite and of opposite sign, yielding a net spin-resolved polarization. To first order in the gradient ∇B, we obtain the modification of the spin polarization, $\mathbf{P}_S = \mathbf{P}_S^{(0)} + \nabla B\, \mathbf{P}_S^{(1)}$. Here, $\mathbf{P}_S^{(0)}$ denotes the intrinsic spin polarization of the Rice–Mele lattice, while $\mathbf{P}_S^{(1)}$ arises from the first-order correction to the eigenstates $|\psi_{-,\sigma}\rangle$. It is worth noting that, $\mathbf{P}_S$ depends on u, $\mathbf{n}$, and ∇B. Consequently, the polarization current in Eq. 2 can be expanded to first order in ∇B, with coefficients λ quantifying the contribution of each system variable to the polarization current. Their explicit form reads,

$$\lambda_{\mathrm{pzsp}} = \frac{\partial(\delta t)}{\partial u} \frac{a}{2\pi} \sum_{\sigma} \int_{-\pi}^{\pi} \Omega^{\tau^z}_{\delta t,\, k}\, dk \tag{8}$$

$$\lambda_{n} = \frac{a}{2\pi} \sum_{\sigma} \int_{-\pi}^{\pi} \Omega^{\tau^z}_{n,\, k}\, dk \tag{9}$$

$$\lambda_{\nabla B} = \frac{a}{2\pi} \sum_{\sigma} \int_{-\pi}^{\pi} \Omega^{\tau^z}_{\nabla B,\, k}\, dk \tag{10}$$

where $\Omega^{\tau^z}_{x,k} \equiv i\left(\langle \partial_x \psi_{-,\sigma}|\, \tau^z\, |\partial_k \psi_{-,\sigma}\rangle - \langle \partial_k \psi_{-,\sigma}|\, \tau^z\, |\partial_x \psi_{-,\sigma}\rangle\right)$ is a generalized Berry curvature with respect to parameter x and crystal momentum k.

From Eq. (6), the magnetic-field gradient $\nabla B\, \hat{\mathbf{z}}$ exerts a torque on $\mathbf{n}$ with two components: one lying in the plane spanned by $\mathbf{n}$ and $\hat{\mathbf{z}}$, which couples directly to the anisotropy field $\mathbf{h_n}$ and governs the dominant dynamics, and one perpendicular to this plane, which is of higher order in the oscillation amplitude and can therefore be neglected. This reduces the problem to an effective one-dimensional dynamics within the plane containing $\mathbf{n}$ and $\hat{\mathbf{z}}$.

To clarify the behavior of the spin current $\mathbf{J}_S$, we analyze its separate contributions, each controlled by a specific λ-parameter. This separation makes it possible to isolate the impact of ∇B on u, on $\mathbf{n}$, and the intrinsic effect of the gradient. Once these contributions are identified and computed, their combined influence is examined together with the classical overdamped equations of motion for u and $\mathbf{n}$, yielding the full dependence of $\mathbf{J}_S$ on the external magnetic-field gradient. This dependence is shown in Fig. 2, where curves for different driving frequencies ω of the oscillating magnetic-field gradient are plotted for regimes below and above the antiferromagnetic resonance frequency of FeOOH, $\omega_{\mathrm{AFMR}} \approx 570$ GHz [52]. In this way, it becomes evident that the spin-current response exhibits hysteretic cycles, thereby giving rise to purely magnetic memristors governed by the effect of the magnetic-field gradient on the spins. To achieve a more complete understanding of these memristive effects, the memristive response, $\mathcal{A} = \oint J_S\, d\nabla B$, was studied as a function of different control parameters of the system under consideration, leading to the results shown in Fig. 3.

5 Discussion

We now present the results of our analysis of the spintronic-magneto-impedictive effect in antiferromagnetic spin chains described by the spin-Rice-Mele Hamiltonian.

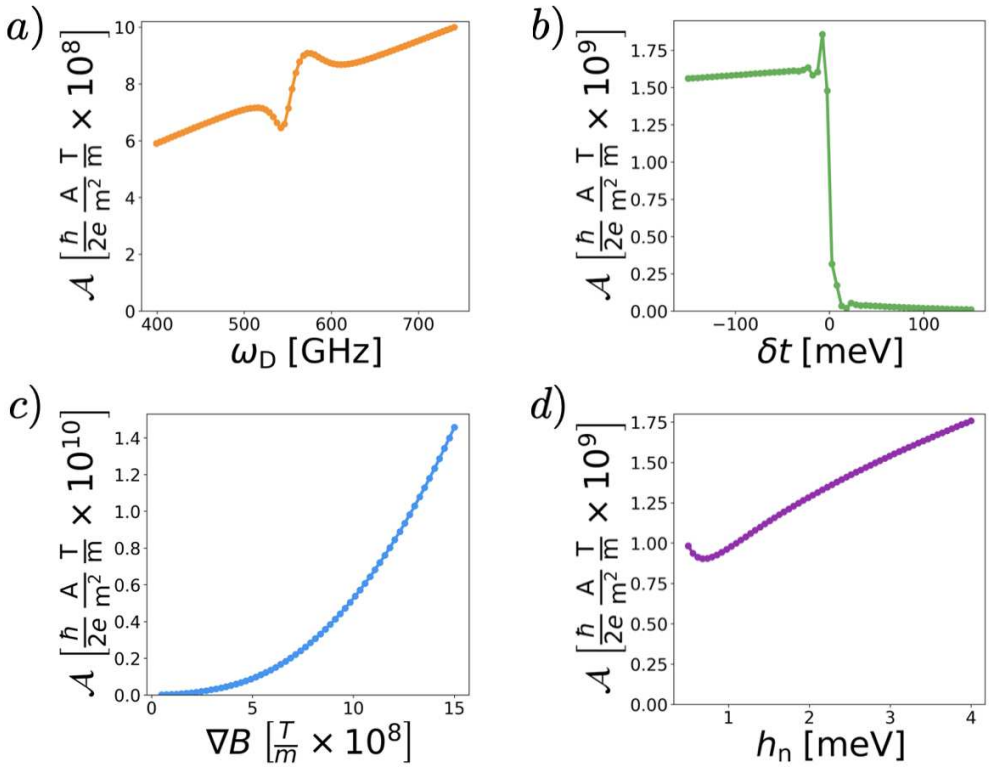


Fig. 3 Plots of the system's memristive effect $\mathcal{A}$ as a function of different control parameters: (a) $\mathcal{A}$ versus the driving frequency ω_D associated with the magnetic-field gradient; (b) $\mathcal{A}$ versus the dimerization δt; (c) $\mathcal{A}$ versus the magnitude of the magnetic-field gradient ∇B; and (d) $\mathcal{A}$ versus the anisotropy parameter h_n. Fixed parameters in each panel: (a) $\delta t = 50$ meV, $\nabla B = 5 \times 10^8$ T/m, and $h_n = 2$ meV; (b) $\omega_D = \omega_{\mathrm{AFMR}}$, $\nabla B = 5 \times 10^8$ T/m, and $h_n = 2$ meV; (c) $\omega_D = \omega_{\mathrm{AFMR}}$, $\delta t = 50$ meV, and $h_n = 2$ meV; (d) $\omega_D = \omega_{\mathrm{AFMR}}$, $\delta t = 50$ meV, and $\nabla B = 5 \times 10^8$ T/m.

The central quantity of interest is the spin current J_S as a function of the applied magnetic-field gradient ∇B, which enters the system through three distinct channels: the piezospintronic coupling λ_{pzsp}, the Néel vector coupling λ_n, and the intrinsic gradient coupling $\lambda_{\nabla B}$. Together, these three contributions govern the full memristive response of the system.

Figure 2 displays the simulated spin-current curves as a function of the magnitude of ∇B for FeOOH chains, computed at driving frequencies of 450, 500, 650, and 800 GHz, spanning regimes both below and above the antiferromagnetic resonance frequency $\omega_{\mathrm{AFMR}} \approx 570$ GHz of FeOOH [52]. The most salient feature of these curves is the appearance of *hysteretic loops* in all frequency regimes, directly establishing the memristive character of the spin-current response. These loops are a direct consequence of the time-dependent state variables—the Néel vector $\mathbf{n}$ and the lattice distortion u—which evolve according to their respective overdamped equations of motion [Eqs. (5) and (6)] and retain information about the history of the applied field gradient. The

system therefore satisfies the defining characteristic of a memristor: its instantaneous response depends not only on the present drive, but on the integrated past dynamics of the internal state.

The shape and area of the hysteretic loops depend sensitively on the driving frequency ω. Below resonance [panels (a)–(b), $\omega = 450$ and 500 GHz], the loops are wide and display a pronounced asymmetry, reflecting the dominant role of the piezospintronic and Néel-vector contributions to the spin current. As the frequency crosses ω_{AFMR} and enters the above-resonance regime [panels (c)–(d), $\omega = 650$ and 800 GHz], the loop morphology changes qualitatively: the curves narrow and the overall magnitude of J_S is reduced, consistent with the overdamped dynamics of $\mathbf{n}$ becoming less responsive to the oscillating gradient at high frequencies. At 800 GHz the loop recovers a larger amplitude, which we attribute to an interplay between the inertial term in the Néel-vector equation of motion and the intrinsic $\lambda_{\nabla B}$ contribution, which becomes dominant when the mechanical degree of freedom u can no longer adiabatically follow the drive. These results confirm that the resonance frequency of the antiferromagnet serves as a natural threshold separating qualitatively different memristive regimes.

To quantify the strength of the memory effect, we compute the memristive response $\mathcal{A} = \oint J_S \, d\nabla B$, defined as the area enclosed by the hysteretic loop in the J_S–∇B plane. A nonzero $\mathcal{A}$ is the direct signature of memristive behavior, and its dependence on system parameters is presented in Fig. 3. Panel (a) shows that $\mathcal{A}$ peaks sharply near ω_{AFMR}, demonstrating that the memory effect is resonantly enhanced and that the antiferromagnetic resonance frequency constitutes an optimal operating point for the device. The peak is relatively narrow in frequency, suggesting that these devices could additionally function as frequency-selective spin-current switches.

Panel (b) of Fig. 3 examines the dependence of $\mathcal{A}$ on the dimerization parameter δt. The memristive response exhibits a strong jump at intermediate values of δt before reaching a saturation regime at large dimerization. This behavior is consistent with the analytical expression for λ_{pzsp} in Eq. (8): a larger bond alternation amplifies the Berry-phase-like integral over the Brillouin zone, yielding a stronger piezospintronic coupling and thus a larger spin polarization response to lattice deformation. This result confirms that dimerization is a key tuning parameter for optimizing device performance, and that materials with a pronounced Peierls-type distortion are the most promising candidates.

Panel (c) shows the dependence of $\mathcal{A}$ on the magnitude of the applied field gradient ∇B. For small gradients the response grows approximately quadratically, as expected from a perturbative treatment in which the leading correction to the loop area is second order in the driving amplitude. At larger ∇B the response saturates and eventually decreases, signaling the onset of nonlinear effects beyond the linear-response regime assumed in the derivation of Eq. (2). The characteristic gradient scale at which this crossover occurs is of order 10^8 T/m. Although large on macroscopic scales, such gradients can be realized at the nanoscale: Zablotskii et al. [49] have measured them near magnetic nanoparticles and sharp scanning-probe tips. For device applications, magnetic force microscopy tips and patterned magnetic nanostructures can already produce highly localized gradients of this magnitude over tens of nanometers. Since our model depends on the gradient integrated along the device, using shorter chains lowers

the total field difference needed. Thus, 10^8 T/m should be viewed as a realistic near-term engineering goal—supported by current trends in nanomagnetics and quantum device fabrication—rather than as a routinely available capability today. This validates the physical relevance of the parameter range used throughout our simulations.

Panel (d) shows how the magnetic anisotropy h_n shapes the memristive response. As h_n increases, the Néel vector stiffens, large fluctuations are suppressed, and the hysteresis loop area shrinks. For very strong anisotropy, $\mathbf{n}$ is effectively pinned to the easy axis, erasing memory. At low anisotropy, freer precession of the Néel vector enriches the dynamics and boosts $\mathcal{A}$. This reveals a trade-off between magnetic stability—needed for state retention—and the spin-current response amplitude, mirroring the stability-plasticity dilemma in neuromorphic systems.

6 Conclusion

The picture that emerges from these results is the following. The applied magnetic-field gradient ∇B simultaneously perturbs the Néel vector, distorts the lattice through the differential Zeeman force on the two sublattices, and directly modifies the electronic eigenstates via the symmetry-breaking term $H_{\nabla B}$ in Eq. (7). Each channel contributes to the spin polarization through the corresponding λ coefficient computed in Eqs. (8)–(10). Because $\mathbf{n}$ and u evolve on their own timescales governed by Eqs. (5)–(6), the system retains a phase lag with respect to the drive, and the combined state $(\mathbf{n}, u)$ traces a closed orbit in state space that does not coincide on the forward and return sweeps—the hallmark of memristive behavior. The spin-current memimpedance $Z_S(\boldsymbol{\alpha}, \omega)$ therefore encodes both the instantaneous electronic response and the cumulative history of the magnetic and mechanical state, realizing a purely spin-based analogue of the memristor originally conceived by Chua [28].

It is worth contrasting the present device with conventional charge-current memristors. In the latter, hysteresis originates from resistive switching driven by ionic migration, phase transitions, or conducting-filament formation, all of which involve substantial Joule dissipation and electromigration damage over repeated cycles [30]. In our antiferromagnetic spin-current memdevice, no net charge flows. To quantify this advantage, we estimate the dissipated power from the two damping channels present in the system: the lattice damping γ in Eq. (5) and the Néel-vector damping α_n in Eq. (6). Evaluating numerically the equations of motion with the material parameters of FeOOH ($\omega_{\mathrm{AFMR}} = 2\pi \times 570$ GHz, $Q = 10$, and $\nabla B = 5 \times 10^8$ T/m), we obtain $P_{\mathrm{lat}} \approx 12$ aW and $P_{\mathrm{Néel}} \approx 2$ pW per unit cell. The total dissipation is dominated by Néel damping at $\sim$2 pW per unit cell, many orders of magnitude below the power typically consumed by conventional charge-based memristive devices ($\sim$ mW per switching event [53]). The absence of stray fields, characteristic of antiferromagnets, further suppresses cross-talk between neighboring devices, a critical advantage for high-density integration [18]. These features position the proposed memdevice as a compelling building block for neuromorphic and unconventional computing architectures that seek to exploit spin degrees of freedom.

We now consider collective excitations in the presence of the magnetic-field gradient. The gradient appears as a field-like torque [Eq. (6)] that can shift the magnon

precession center or resonantly excite magnons. Sustaining large magnon currents, however, would require an anti-damping-like torque—missing in our system—as found in heavy-metal/magnetic-insulator bilayers [54] or spin-Seebeck setups. In our device, there is no electrical current and negligible power dissipation (see above), so thermal fluctuations are minimal and magnonic or phononic effects are not expected to be important. Instead, we focus on adiabatic changes of the global spin-polarized electronic structure, in the spirit of the modern theory of polarization, where the spin current follows from Berry-curvature terms given in Eqs. (8)–(10).

Although our analysis focused on FeOOH as a concrete example, the theoretical framework applies to any $\mathcal{PT}$-invariant piezospintronic antiferromagnet described by the spin-Rice-Mele Hamiltonian, including the one-dimensional MoX_3 (X = Cl, Br, I) family [46]. The tunability of the resonance frequency, dimerization strength, and magnetic anisotropy across these materials class offers broad flexibility for targeting specific operational frequency windows and for optimizing memory performance to meet given device requirements. We anticipate that recent progress in the fabrication and characterization of low-dimensional magnetic insulators [25, 26] will enable experimental realization and testing of these predictions in the near term.

Acknowledgements. A.S.N. and R.E.T. acknowledge funding from Fondecyt Regular 1230515 and 1230747, respectively. This work was funded by ANID CEDENNA CIA 250002

References

[1] Wang, K.: Spintronics. Wiley Series in Materials for Electronic & Optoelectronic Applications. John Wiley & Sons, Nashville, TN (2025)

[2] Dey, P., Roy, J.N.: Spintronics: Fundamentals and Applications. Springer, Cham, Switzerland (2021)

[3] Maekawa, S., Valenzuela, S.O., Saitoh, E., Kimura, T. (eds.): Spin Current, 2nd edn. Series on Semiconductor Science and Technology. Oxford University Press, London, England (2017)

[4] Maekawa, S., Kikkawa, T., Chudo, H., Ieda, J., Saitoh, E.: Spin and spin current—from fundamentals to recent progress. Journal of Applied Physics **133**(2) (2023) https://doi.org/10.1063/5.0133335

[5] Johnson, M.: Spin Injection, pp. 329–354. Springer, ??? (2017). https://doi.org/10.1007/978-3-319-65436-2_10

[6] Sinova, J., Valenzuela, S.O., Wunderlich, J., Back, C.H., Jungwirth, T.: Spin hall effects. Reviews of Modern Physics **87**(4), 1213–1260 (2015) https://doi.org/10.1103/RevModPhys.87.1213

[7] Takahashi, S.: In: Xu, Y., Awschalom, D.D., Nitta, J. (eds.) Physical Principles of Spin Pumping, pp. 1445–1480. Springer, Dordrecht (2016). https://doi.org/10.

1007/978-94-007-6892-5_51

[8] Uchida, K., Takahashi, S., Harii, K., Ieda, J., Koshibae, W., Ando, K., Maekawa, S., Saitoh, E.: Observation of the spin seebeck effect. Nature **455**(7214), 778–781 (2008) https://doi.org/10.1038/nature07321

[9] Shao, Q., Li, P., Liu, L., Yang, H., Fukami, S., Razavi, A., Wu, H., Wang, K., Freimuth, F., Mokrousov, Y., Stiles, M.D., Emori, S., Hoffmann, A., Akerman, J., Roy, K., Wang, J.-P., Yang, S.-H., Garello, K., Zhang, W.: Roadmap of spin–orbit torques. IEEE Transactions on Magnetics **57**(7), 1–39 (2021) https://doi.org/10.1109/tmag.2021.3078583

[10] Ji, Y., Hoffmann, A., Jiang, J.S., Pearson, J.E., Bader, S.D.: Non-local spin injection in lateral spin valves. Journal of Physics D: Applied Physics **40**(5), 1280–1284 (2007) https://doi.org/10.1088/0022-3727/40/5/s13

[11] Driel, H.M., Sipe, J.E., Smirl, A.L.: Coherence control of electron spin currents in semiconductors. physica status solidi (b) **243**(10), 2278–2284 (2006) https://doi.org/10.1002/pssb.200668021

[12] Desmarais, J.K., Maul, J., Civalleri, B., Erba, A., Vignale, G., Pittalis, S.: Spin currents via the gauge principle for meta-generalized gradient exchange-correlation functionals. Physical Review Letters **132**(25) (2024) https://doi.org/10.1103/physrevlett.132.256401

[13] Amin, V.P., Li, J., Stiles, M.D., Haney, P.M.: Intrinsic spin currents in ferromagnets. Physical Review B **99**(22) (2019) https://doi.org/10.1103/physrevb.99.220405

[14] Liu, Q., Lin, X., Shaked, A., Nie, Z., Yu, G., Zhu, L.: Efficient generation of out-of-plane polarized spin current in polycrystalline heavy metal devices with broken electric symmetries. Advanced Materials **36**(40) (2024) https://doi.org/10.1002/adma.202406552

[15] Zhang, S., Fert, A.: Conversion between spin and charge currents with topological insulators. Physical Review B **94**(18) (2016) https://doi.org/10.1103/physrevb.94.184423

[16] Takahashi, S., Maekawa, S.: Spin current in metals and superconductors. Journal of the Physical Society of Japan **77**(3), 031009 (2008) https://doi.org/10.1143/jpsj.77.031009

[17] Baltz, V., Manchon, A., Tsoi, M., Moriyama, T., Ono, T., Tserkovnyak, Y.: Antiferromagnetic spintronics. Reviews of Modern Physics **90**(1) (2018) https://doi.org/10.1103/revmodphys.90.015005

[18] Jungwirth, T., Marti, X., Wadley, P., Wunderlich, J.: Antiferromagnetic spintronics. Nature Nanotechnology **11**(3), 231–241 (2016) https://doi.org/10.1038/nnano.2016.18

[19] Dal Din, A., Amin, O.J., Wadley, P., Edmonds, K.W.: Antiferromagnetic spintronics and beyond. npj Spintronics **2**(1) (2024) https://doi.org/10.1038/s44306-024-00029-0

[20] Lebrun, R., Ross, A., Bender, S.A., Qaiumzadeh, A., Baldrati, L., Cramer, J., Brataas, A., Duine, R.A., Kläui, M.: Tunable long-distance spin transport in a crystalline antiferromagnetic iron oxide. Nature **561**(7722), 222–225 (2018) https://doi.org/10.1038/s41586-018-0490-7

[21] Das, S., Ross, A., Ma, X.X., Becker, S., Schmitt, C., Duijn, F., Galindez-Ruales, E.F., Fuhrmann, F., Syskaki, M.-A., Ebels, U., Baltz, V., Barra, A.-L., Chen, H.Y., Jakob, G., Cao, S.X., Sinova, J., Gomonay, O., Lebrun, R., Kläui, M.: Anisotropic long-range spin transport in canted antiferromagnetic orthoferrite yfeo3. Nature Communications **13**(1) (2022) https://doi.org/10.1038/s41467-022-33520-5

[22] Nunez, Alvaro S.: Theory of the piezo-spintronic effect. Solid State Communications **198**, 18–21 (2014) https://doi.org/10.1016/j.ssc.2013.10.018

[23] Ulloa, C., Troncoso, R.E., Bender, S.A., Duine, R.A., Nunez, A.S.: Piezospintronic effect in honeycomb antiferromagnets. Physical Review B **96**(10) (2017) https://doi.org/10.1103/physrevb.96.104419

[24] Liu, Z., Feng, Z., Yan, H., Wang, X., Zhou, X., Qin, P., Guo, H., Yu, R., Jiang, C.: Antiferromagnetic piezospintronics. Advanced Electronic Materials **5**(7) (2019) https://doi.org/10.1002/aelm.201900176

[25] Saez, G., Vergara, P., Castro, M., Allende, S., Nunez, A.S.: Ferrospintronic order in noncentrosymmetric antiferromagnets: An avenue toward spintronic-based computing, data storage, and energy harvesting. physica status solidi (RRL) – Rapid Research Letters **19**(3) (2024) https://doi.org/10.1002/pssr.202400292

[26] Chen, Y., Ji, J., Hong, L., Wan, X., Xiang, H.: Generation of pure spin current with insulating antiferromagnetic materials. Physical Review Letters **135**(14) (2025) https://doi.org/10.1103/n8d2-hjnd

[27] Castro, M., Mancilla, B., Wolff, F., Nunez, A.S.: Quantized piezospintronic effect in moiré systems. arXiv (2025) https://doi.org/10.48550/ARXIV.2510.03841

[28] Chua, L.: Memristor-the missing circuit element. IEEE Transactions on Circuit Theory **18**(5), 507–519 (1971) https://doi.org/10.1109/tct.1971.1083337

[29] Chua, L., Sirakoulis, G.C., Adamatzky, A. (eds.): Handbook of Memristor

Networks, 2019 edn. Springer, Cham, Switzerland (2019)

[30] Mazumder, P., Kang, S.M., Waser, R.: Memristors: Devices, models, and applications [scanning the issue]. Proceedings of the IEEE **100**(6), 1911–1919 (2012) https://doi.org/10.1109/jproc.2012.2190812

[31] Adamatzky, A., Chua, L. (eds.): Memristor Networks, 2014 edn. Springer, Basel, Switzerland (2013)

[32] Tetzlaff, R. (ed.): Memristors and Memristive Systems, 2014 edn. Springer, New York, NY (2013)

[33] Sort, J., Everschor-Sitte, K., Ielmini, D., Lira-Cantu, M.: Energy-efficient memory materials. APL Materials **13**(10) (2025) https://doi.org/10.1063/5.0300514

[34] Latorre, M., Barrera, G., Troncoso, R.E., Nunez, A.S.: A simple model for an intrinsic piezoelectric memristor. physica status solidi (RRL) – Rapid Research Letters **20**(6), 70197 (2026) https://doi.org/10.1002/pssr.70197 https://onlinelibrary.wiley.com/doi/pdf/10.1002/pssr.70197

[35] Wakrim, T., Vallée, C., Gonon, P., Mannequin, C., Sylvestre, A.: From memristor to memimpedance device. Applied Physics Letters **108**(5), 053502 (2016) https://doi.org/10.1063/1.4941231

[36] MacVittie, K., Katz, E.: Electrochemical system with memimpedance properties. The Journal of Physical Chemistry C **117**(47), 24943–24947 (2013) https://doi.org/10.1021/jp409257v

[37] Vidal-Silva, N., Aguilera, E., Roldán-Molina, A., Duine, R.A., Nunez, A.S.: Magnon polarons induced by a magnetic field gradient. Physical Review B **102**(10) (2020) https://doi.org/10.1103/physrevb.102.104411

[38] Pal, S., Pal, P.K., Fabiha, R., Bandyopadhyay, S., Barman, A.: Acousto-plasmo-magnonics: Coupling spin waves with hybridized phonon-plasmon waves in a 2d artificial magnonic crystal deposited on a plasmonic material. Advanced Functional Materials **33**(37) (2023) https://doi.org/10.1002/adfm.202304127

[39] Majumder, S., Drobitch, J.L., Bandyopadhyay, S., Barman, A.: Formation of binary magnon polaron in a two-dimensional artificial magneto-elastic crystal. NPG Asia Materials **15**(1) (2023) https://doi.org/10.1038/s41427-023-00499-4

[40] Bandyopadhyay, S.: Magnetic Straintronics, 2022 edn. Synthesis Lectures on Engineering, Science, and Technology. Springer, Cham, Switzerland (2022)

[41] Jackson, J.D.: Classical Electrodynamics, 3rd edn. John Wiley & Sons, Nashville, TN (1998)

[42] Griffiths, D.J.: Introduction to Electrodynamics, 5th edn. Cambridge University

Press, Cambridge, England (2023)

[43] Zangwill, A.: Modern Electrodynamics. Cambridge University Press, Cambridge, England (2012)

[44] Vergara, P., Sáez, G., Castro, M., Allende, S., Nunez, A.S.: Emerging topological multiferroics from the 2d rice-mele model. npj 2D Materials and Applications **8**(1) (2024) https://doi.org/10.1038/s41699-024-00478-5

[45] Saez, G., Castro, M.A., Allende, S., Nunez, A.S.: Model for nonrelativistic topological multiferroic matter. Physical Review Letters **131**(22) (2023) https://doi.org/10.1103/physrevlett.131.226801

[46] Mella, A., Suárez-Morell, E., Nunez, A.S.: Magnetic spirals and biquadratic exchange in 1d mox_3 spin chains. Journal of Magnetism and Magnetic Materials **594**, 171882 (2024) https://doi.org/10.1016/j.jmmm.2024.171882

[47] Landau, L.D., Lifshitz, E.M.: Mechanics, 3rd edn. Course of Theoretical Physics, vol. 1. Butterworth-Heinemann Limited, Oxford (1976)

[48] Yuan, H.Y., Yuan, Z., Duine, R.A., Wang, X.R.: Recent progress in antiferromagnetic dynamics. EPL (Europhysics Letters) **132**(5), 57001 (2021) https://doi.org/10.1209/0295-5075/132/57001

[49] Zablotskii, V., Polyakova, T., Lunov, O., Dejneka, A.: How a high-gradient magnetic field could affect cell life. Scientific Reports **6**(1) (2016) https://doi.org/10.1038/srep37407

[50] Vanderbilt, D.: Berry Phases in Electronic Structure Theory. Cambridge University Press, Cambridge, England (2018)

[51] Sundaram, G., Niu, Q.: Wave-packet dynamics in slowly perturbed crystals: Gradient corrections and berry-phase effects. Physical Review B **59**(23), 14915–14925 (1999) https://doi.org/10.1103/PhysRevB.59.14915

[52] Chou, S.G., Stutzman, P.E., Provenzano, V., McMichael, R.D., Surek, J., Wang, S., Plusquellic, D.F., Garboczi, E.J.: Using terahertz waves to identify the presence of goethite via antiferromagnetic resonance. Applied Magnetic Resonance **48**(6), 559–569 (2017) https://doi.org/10.1007/s00723-017-0884-y

[53] Yoon, J.H., Ham, W., Park, K.J., Namgung, S.D., Song, M.-K., Kwon, J.-Y.: Ultralow-power peptide-based memristor enabled by emulation of proton-mediated synaptic signaling. Small Methods **9**(12), 01472 (2025) https://doi.org/10.1002/smtd.202501472 https://onlinelibrary.wiley.com/doi/pdf/10.1002/smtd.202501472

[54] Chen, Y.-T., Takahashi, S., Nakayama, H., Althammer, M., Goennenwein, S.T.B.,

Saitoh, E., Bauer, G.E.W.: Theory of spin hall magnetoresistance. Phys. Rev. B **87**, 144411 (2013) https://doi.org/10.1103/PhysRevB.87.144411